Realization of High Aspect Ratio Anti-reflection Structures via Laser Irradiation inside Liquids

Yi Zhu[1], Rui Zhou[*12], and Minghui Hong[*1]

[1] *Pen-Tung Sah Institute of Micro-Nano Science and Technology, Xiamen University, Xiamen, 361005, China*
[2] *Innovation Laboratory for Sciences and Technologies of Energy Materials of Fujian Province (IKKEM), Xiamen, 361005, China*
[*]*Corresponding author's emails: rzhou2@xmu.edu.cn; elehmh@xmu.edu.cn*

Anti-reflection structures (ARS) in micro/nano-scales provide remarkable opportunities for broadband and omnidirectional anti-reflection performance. In this work, laser-induced surface structures at a high aspect ratio of 3.4 and a period of 50 μm are firstly created on crystalline silicon wafers by nanosecond pulsed laser ablation in air. Meanwhile, a high aspect ratio of 5.0 structures for enhanced light trapping are realized via laser ablation inside water. Such enhancement is attributed to the limitation of plasma inside water. The processing rate is increased by 2.34 times with the localized chemical etching inside NaOH solution. The average reflection of 3.28% is achieved from 380 to 780 nm, 15% lower than laser ablation in air. Laser ablation with the liquid assistance provides a new method to generate high aspect ratio ARS.
DOI: 10.2961/jlmn.2023.01.2008
Keywords: laser ablation, anti-reflection structures, high aspect ratio, light trapping, liquid assistance

1. Introduction

As a semiconductor material, silicon (Si) is widely applied in many fields, such as solar cells [1], photodetectors, and infra-red stealthy camouflage. Nevertheless, more than 30% of optical losses on silicon surface due to high refractive index (RI) ≈3.4 at the visible light range. Little light absorption above ~1100 nm limits the improvement of optoelectronic device performance [2, 3]. Hence, great efforts have been made to reduce the reflection and enhance the light absorption by ARS.

Light trapping and thin film coatings are the main ways to engineer Si surfaces for anti-reflection. Thin film coatings with the appropriate design of thickness and RI in each layer are used for high anti-reflection performance[4]. There are several challenges, including material selection and the mismatch in the thermal properties of different materials. The enhanced absorption using light trapping has more advantages and also studied in various fields of optics [5]. This is because the light-trapping structures can achieve better broadband and omnidirectional optical performances.

In the last few decades, inspired by natural biological materials with sophisticated light-trapping structures, a great number of the ARS have been prepared to improve optical performances at the interface between air and substrates [6-10]. The ARS fabrication with broadband and omnidirectional anti-reflection performance is realized [11-16]. However, these approaches are time-consuming or complicated, which make them hard to be mass produced over a large scale. It is necessary to find a new fabrication method which is simple, high-speed, and suitable for practical applications.

Laser ablation [17, 18] is an advanced process to obtain easy-to-fine-tune sizes and surface morphologies. It is a key to modulate structures at a high aspect ratio for anti-reflection. Yang J et al. realized the fabrication of broadband anti-reflection Si surfaces by laser micro/nano-processing [16]. The enhancement of laser ablation efficiency in various liquids has also been studied. Zhu S et al. found that the laser ablation rate of Si can be highly enhanced by a water layer of 1.1 mm thick [19]. Maack P et al confirmed that laser ablation inside liquid allows for a significant reduction in particles' redeposition [20]. Zhai Z et al. compared the processing results of micro-holes via nanosecond pulse laser in air and water environments [21]. Hong M et al. demonstrated the materials removal rate for laser ablation inside KOH solution is twice as high as that inside water at a cooled liquid environment (temperature ~10°C) [22]. The enhancement mechanism was also explored. Lam J et al. examined the initial growth and collapse stages of bubbles induced by laser ablation inside water, pure ethanol (96%), and isopropanol (99.5%) [23]. Shaheen M. E. et al. found the ablation rate of brass is higher inside water and ethanol than that in air with clean surfaces and little debris re-deposition [24]. Hayat A et al. proved that the difference in surface morphology is attributed to cooling, confinement, and shielding effects [25]. Meanwhile, to the best of our knowledge, no efforts are made so far to assess the ARS on Si surface fabricated by nanosecond-laser ablation inside liquids.

In this work, laser-induced structures on Si surface at a period of 50 μm and aspect ratio of 3.4 are manufactured on crystalline silicon wafer by nanosecond-laser ablation in air. A 1.5-times higher aspect ratio of the ARS for enhanced light-trapping is realized via laser ablation inside liquids.

The average reflection in the visible spectrum is 15% lower with the water assistance. Inside NaOH solution, the average reflection is lower by 5.43% than that in air and the processing efficiency is much improved.

2. Experimental

Laser processing of 525±25 μm thick polished monocrystalline Si wafers (P/111, <0.02 ohm-cm) is performed in air, inside water, and NaOH solution (wt=20%) using 1064 nm/200 ns fiber laser (YDFLP-E-30-LP-S, JPT) as shown in Fig. 1a. Periodic structures are produced by focusing the laser beam in air or through an 1-mm thick liquid layer onto Si surfaces. A galvo is used to scan over an area of 110 × 110 mm^2 at a spot size of 30 μm (Fig. 1b). Figure 1c shows the schematic of periodic structures fabricated by laser ablation.

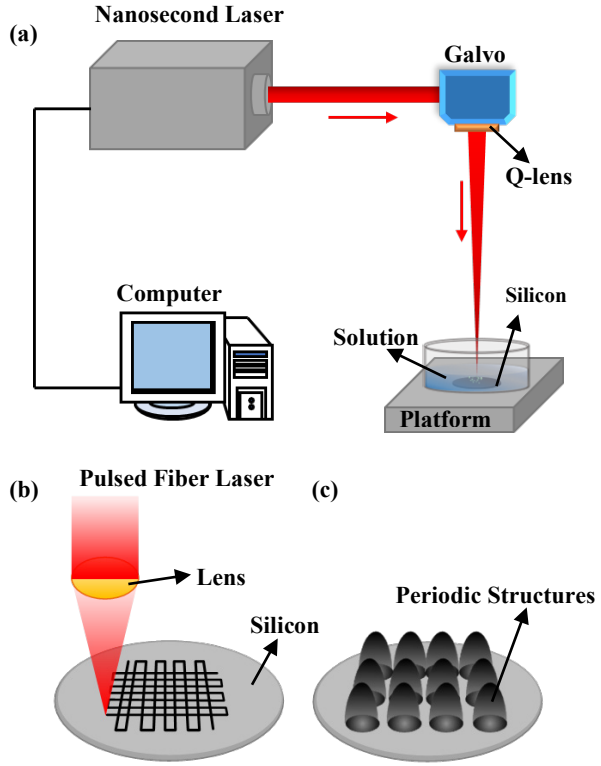

Fig. 1 Schematic of (a) laser processing silicon wafer inside liquid, (b) pulse fiber laser scanning for periodic surface structures fabrication, (c) Si anti-reflection structures morphology.

The oblique view (38° tilt angle) of the laser-processed Si surface is taken by scanning electric microscope (SEM, SUPRA55 SAPPHIRE, ZEISS) at a primary electron energy of 20 kV. Energy Dispersive X-ray Spectroscopy (EDS) is used to detect the elements of the sample. The surface morphology (width and height) of the ablated structures is inspected by a confocal laser scanning microscope (CLSM, VK-X1000, KEYENCE). Reflection spectrum from 380 to 780 nm is measured by a UV/VIS/NIR spectrometer (LAMBDA 1050, Perkin Elmer) with a 150 mm integrating sphere.

3. Results and Discussion

To optimize the anti-reflection performance of the ARS, different processing parameters for laser ablation, including scanning gap, scanning speed, laser power, and scanning number, are tuned in air. As the scanning gap increases from 30 to 70 μm (the scanning speed is 500 mm/s, the laser power 15 W, and the scanning number 5), the morphologies of the silicon surface are changed greatly. When the scanning gap is equal to the spot size (30 μm), no obvious structure is generated. Some energy is converted to heat when a pulsed nanosecond laser is applied to silicon surface in air. The heat from laser ablation is accumulated and spread around. Then the heat affected zone (HAZ) is generated, which expends the crater area. In this case, the crater size is larger than the spot size so that the area of laser ablation is overlapped. Therefore, it is a key to increase the scanning gap to fabricate anti-reflection structures.

The height and average reflection of the silicon surface at different scanning gaps are characterized in Fig. 2a. Periodic surface cone microstructures are formed at a scanning gap of 50 μm. As the scanning gap is larger than 50 μm, the truncated pyramid of silicon surface structures is obtained. It is found that the period of the structure is equal to the scanning gap. A lower reflection is measured at a 50 μm scanning gap when the structures are 34 μm height with a corresponding 1.36 aspect ratio. The laser processed areas are good at light trapping. Therefore, the cone microstructures are more beneficial to the light anti-reflection.

The dimensions of the arrayed structures made by laser ablation are much larger than light wavelength. Ray tracing model of light trapping used to illustrate the mechanism of anti-reflection in microstructure arrays is shown in Fig. 3. In COMSOL simulation, the cone structures are defined as the default silicon material and the wavelength of incident light is 660 nm. Different aspect ratio cone structures are simulated while the diameters are kept as 50 μm. When the light encounters air-silicon interface, it is absorbed, refracted and reflected. The more light is reflected, the more light energy is lost. As shown in Fig. 3a, for the vertical plane incident light, there are three reflections between the cones whose aspect ratio is 2. Each reflection provides a chance to absorb light, thus acting as anti-reflection effect. To explore the effect of structural aspect ratio on anti-reflection performance, incident light paths in cones of the same diameter with different heights are simulated. As the aspect ratio changes from 4 (Fig. 3b) to 6 (Fig. 3c), the number of reflections between the cone structures increases from 6 to 9. The incident light is trapped inside the gaps of a high aspect ratio microstructure array. The multiple reflection of light on the inner surface of the microstructure increases optical path length, which further reduces reflection and improves the light absorption [26]. Thus, the aspect ratio of individual units is larger, the number of reflections is more, which leads to a lower reflection in the visible range.

Laser power determines ablation depth while the scanning speed and scanning number fix pulse numbers acting on the ablation zone. The crater height can be deepened by modulating these parameters with a 50 μm scanning gap. Figure 2b shows that a lower reflection on Si surfaces by laser ablation in air is obtained for 300 mm/s speed, but structures on the surface are irregular. When scanning speed is 500 mm/s, the average surface reflection is similar to the result at 300 mm/s and the uniform structure are higher.

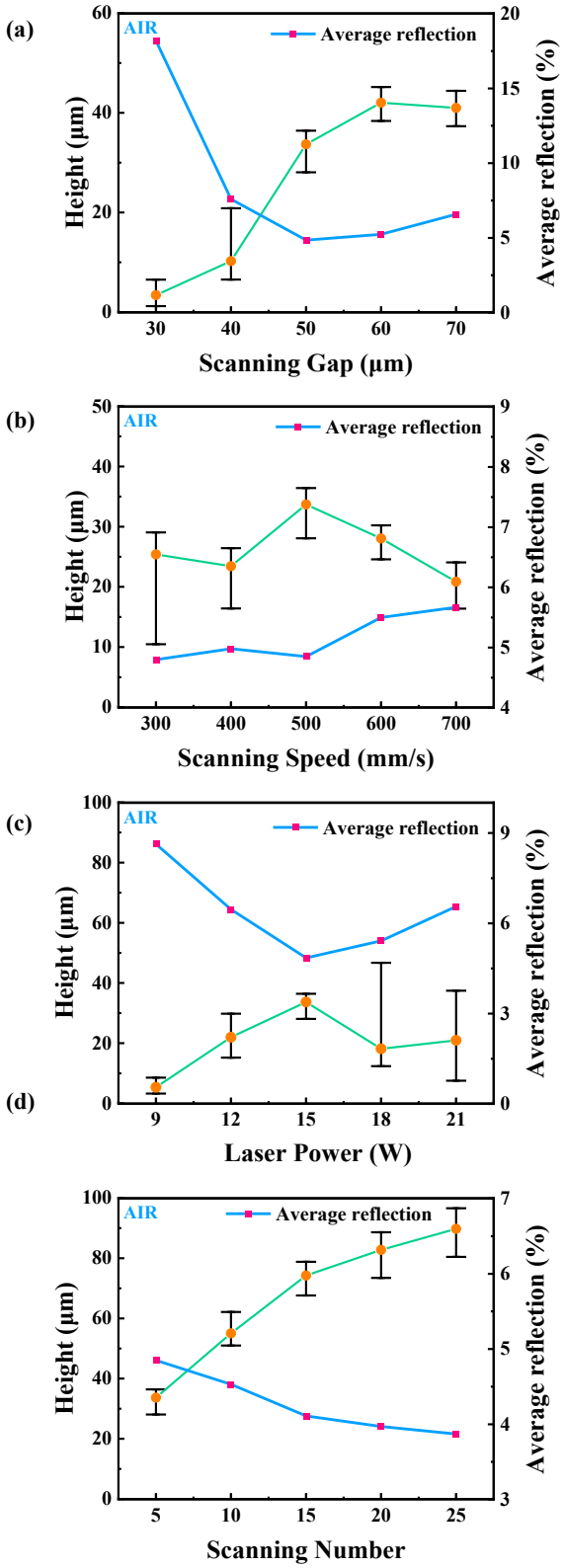

Fig. 2 Plots of relationship between (a) scanning gap, (b) scanning speed, (c) laser power, and (d) scanning number and the heights or the average reflection of the ARS on Si surfaces by laser ablation in air.

The relationship between laser power from 9 to 21 W and structures fabricated via laser irradiation in air is shown in Fig. 2c. Interestingly, the reflection is lower and structures are higher and more uniform at a laser power of 15 W. As the laser power increases to 18 W or 21 W, the structures on the silicon surfaces become disorganized. These results are different from our expectation. In theory, for a slower speed or a higher power, a deeper crater is generated by laser ablation. In fact, the HAZ around the structures not only enhances depth but also damages structural integrity, which restricts the ARS fabrication.

To increase the aspect ratio of ARS, the scanning number is optimized at a scanning gap of 50 μm, scanning speed of 500 mm/s, and laser power 15W. The aspect ratio and reflection of morphologies on the silicon surface generated via laser ablation in air at the scanning number of 5, 10, 15, 20, and 25 are evaluated, as shown in Fig. 2d. The height of the cone microstructures is closely related to scanning number, while average reflection is reduced with scanning number increasing. With the further increasing of scanning number, these changes gradually saturate. As the scanning number is 25, periodic cone microstructures with an aspect ratio of 3.4 are obtained and the average surface reflection with the ARS is reduced to 3.87% in the visible light spectrum.

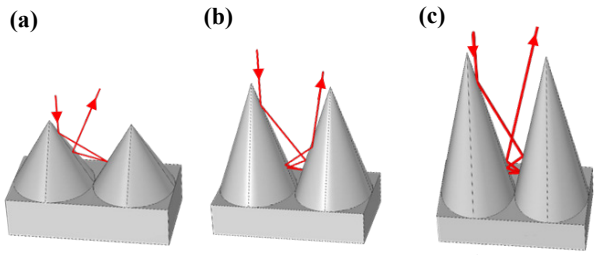

Fig. 3 Ray tracing of light trapping. The aspect ratio of the cone is (a) 2, (b) 4, and (c) 6, reflectively.

It is a key to achieve higher crater depth and better anti-reflection performance. Different processing environments are used to reduce the range of HAZ during laser ablation. Water is a good medium for heat dissipation and the enhancement of laser ablation inside water has been confirmed. It is also an efficient method to avoid the collapse of a structure due to excessive laser ablation. Using the same laser parameter optimization method as in air, high aspect ratio anti-reflection structures are fabricated via laser ablation at a 65 μm scanning gap, 300 mm/s scanning speed, 30 W laser power, and 25 scanning number inside 1-mm thick water layer. Figure 4a shows with the increase of scanning number, the height of the ARS is higher and the average reflection on Si surface is reduced. A low average reflection of 3.28%, corresponding anti-reflection structures with 5.0 aspect ratio, is achieved at a scanning number of 25.

As shown in Fig. 4b, the three-dimensional (3D) morphology of microstructures on silicon surfaces formed inside water at these laser parameters is observed by CLSM. The 3D morphology is high aspect ratio conical array structures with a 65 μm period. To analyze the surface roughness of the structures, the SEM images of the sample surfaces after the laser processing inside water and air are shown in Figs. 4c & d. There are two different features among these laser ablated surfaces. One is the size of microstructures formed on these surfaces. The other is the presence of debris on the surfaces processed in air while

nearly no debris is found on the surfaces via laser ablation inside water. The existence of the debris makes the surface rougher. The assistance of water layer reduces the debris generation and limits the splash. The fluidity of a liquid accounts for the further removal of the formed debris, also resulting in clean ablation edges. Meanwhile, the elements of the fabricated surface are measured by EDS. There are only oxygen and silicon two elements. The mass fraction of oxygen is 24.28% for the laser ablation in air (Fig. 4d) and is only 15.19% for the ablation in water (Fig. 4c). Oxygen content of the fabricated surface are significantly reduced with the assistance of water. Hence, laser ablation with the water assistance results in better laser processing quality compared to that in air.

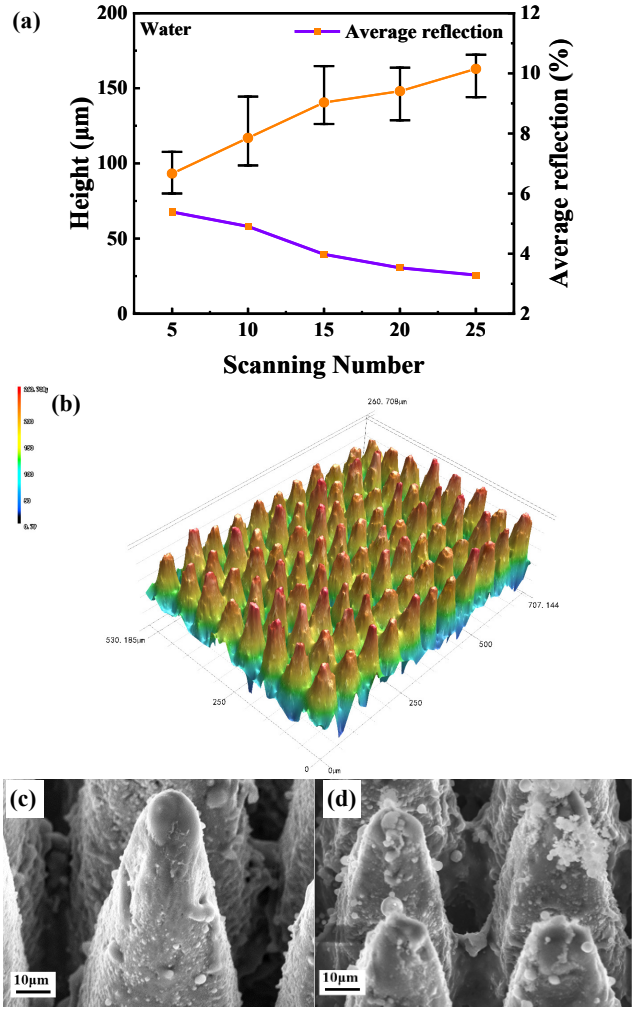

Fig. 4 (a) Plots of relationship between scanning number and the height or the average reflection of the ARS by laser ablation in water. (b) & (c) CLSM and SEM images of periodic surface microstructures formed inside water at 65 μm scanning gap, 300 mm/s scanning speed, 30 W laser power, and 25 scanning number. (d) SEM images of the ARS via laser ablation in air (50 μm scanning gap, 500 mm/s scanning speed, 15 W laser power, and 25 scanning number).

The difference of the microstructure sizes can be explained by the high temperature and high pressure of the limited plasma and more effective cooling inside water [27, 28]. As Fig. 5a shows, when laser pulses provide high enough fluences on Si surface, the electrons reach high-excited states due to the inverse-bremsstrahlung process [29]. After electrons lattice collisions and energy transfer, the dense clouds of excited ions and atoms are generated [30]. The plasma plume then develops into a mixture vapor containing ions, atoms, and electrons, as shown in Fig. 5b. With the continuous absorption of laser pulse energy in the later period, the plasma plume undergoes isothermal expansion, and the pressure and temperature increase at a fast rate. After laser pulse is terminated, the plasma plume expands adiabatically and has the characteristics of high pressure and high temperature [31]. The pressure of the plasma plume is demonstrated to be a few Gigapascals and the temperature can reach up to thousands of Kelvin [28]. This expansion lasts for around 100 μs and then shrinks up to collapse. Meanwhile, due to the higher heat capacity and thermal conductivity of water, the plasma plume cools down much faster than that in air and the HAZ is minimized so that lower scanning speed, and higher laser power can be applied to fabricate high aspect ratio anti-reflection structures. It can be concluded that laser ablation inside water induces a plasma plume with a higher temperature and high pressure as well as a stronger shockwave and a higher impact force, compared with that in air. These plasma species are ejected out from Si surface anisotropically during laser ablation and the strong recoil pressure is generated during the plasma formation [32]. The molten areas are pushed aside by the strong shock wave inside water. These factors result in the expanded ablation-craters which is 15 μm wider than that in air, and the efficiency of materials removal increases [31].

Meanwhile, because of the strong effect of plasma, the thickness t (Fig. 5b) of the water layer which is the distance between the upper silicon surface and the air-water interface is a key factor. When t is small, the water layer is not effective in limiting plasma expansion, the surface tension becomes smaller at high temperature. Considering the absorption and refraction of laser through the water layer, the laser energy loss is much greater than the enhancement effect of plasma when t is too thick. Based on the above two factors, the best enhancement of laser ablation effect is achieved under an 1-mm thick water layer.

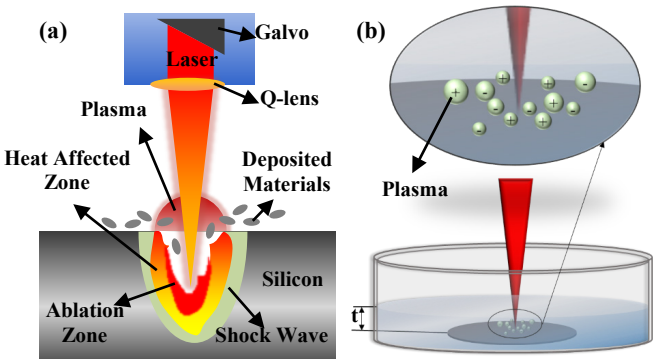

Fig. 5 (a) Schematic of pulsed laser ablation for microstructures generation and their materials deposition on silicon substrate. (b) Diagram of plasma generated via laser ablation inside liquid.

To further investigate the fabrication of high aspect ratio anti-reflection structures by laser, a NaOH solution with a 20% mass fraction (wt=20%) is employed as the processing environment.

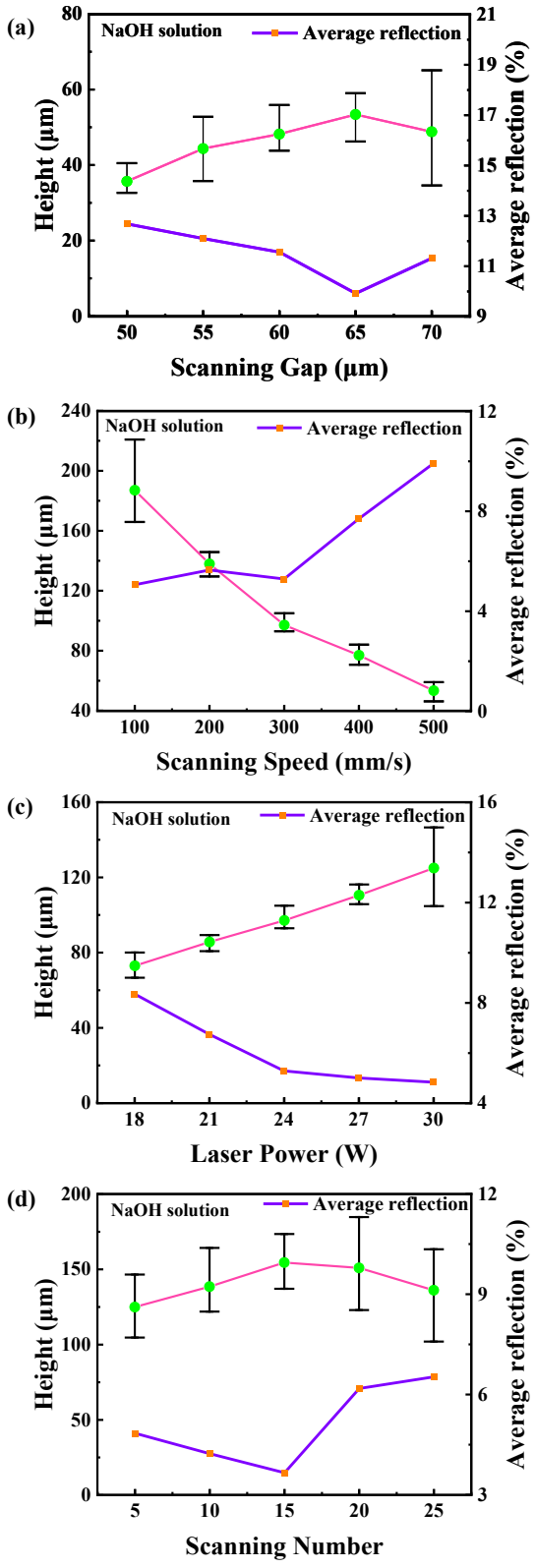

Fig. 6 Plots of relationship between (a) scanning gap, (b) scanning speed, (c) laser power, and (d) scanning number and the heights or the average reflection of the ARS on Si surfaces by laser ablation in wt=20% NaOH solution.

As Fig. 6a shows, it is found that 65 μm is the best scanning gap to fabricate anti-reflection structures inside NaOH solution at the scanning speed of 500 mm/s, the laser power of 24 W, and the scanning number of 5.The aspect ratio of ARS is 1.63 and the average reflection is 9.92%. The limited plasma is also generated inside an 1-mm thickness NaOH solution, resulting in a wider and deeper crater. Figures 6b & c show that the scanning speed of 300 mm/s and laser power of 30 W are the best laser processing parameters to generate high aspect ratio structures inside NaOH solution. The height of structures changes significantly with the increasement of scanning speed. At the speed of 100 mm/s, the average reflection of silicon surface is lower with high but irregular ARS. However, the ARS fabricated via laser ablation inside NaOH solution are uniform at 300 mm/s speed and the average reflection is as low as that at 100 mm/s. The structures height rises linearly as change laser power increases from 18 W to 30 W. The average reflection decreases continuously and reaches saturation.

The height and performance of ARS are also measured as the scanning number increases from 5 to 25 at the scanning gap of 65 μm, scanning speed of 300 mm/s, and laser power 30W, as shown in Fig. 6d. The best scanning number is 15 inside NaOH solution which is reduced by 40% than that in air and inside water. The aspect ratio of ARS is 4.8. A more interesting thing is that as the scanning number increases more than 15, the height of structures is reduced, and the reflection is increased. The minimum average reflection is 3.66% lower than that in air (4.11%, Fig. 2d) and water (3.98%, Fig. 4a) at the scanning number of 15. Furthermore, the optimized average reflection is lower by 5.43% than that in air (3.87%, Fig. 2d). The processing rate is defined as the aspect ratio divided by the scanning number and is increased by 2.34 times for laser ablation in NaOH solution than in air.

Enhancement of the fabrication inside NaOH solution is attributed to both the strong limitation of the plasma plume and the assistance of localized chemical etching. The etching of silicon involves the hydroxide ion-catalyzed reaction of silicon to generate hydrogen and silicate [33]. The chemical reactions between the liquid and silicon interface take place as follows

$$Si+4H_2O \xrightarrow{OH^{-1}} Si(OH)_4+2H_2\uparrow. \quad (1)$$

The hydroxide ion is an important reactant in the overall reaction. More importantly, the reaction rate is accelerated due to high temperature around the plasma induced by laser. Arrhenius proposed an equation for the dependence of the rate k of a chemical reaction on temperature T[34]:

$$k = A\exp(-Ea/(k_B T)). \quad (2)$$

Where A is the pre-exponential factor, Ea the activation energy, and k_B the Boltzmann constant. Equation 2 reveals that the rate constant k is an exponential multiplied by temperature T. It means that the reactions are much more intensive at a higher temperature. Laser ablation provides a high temperature environment for chemical reactions to increase the processing efficiency. Due to the strong chemical reactions as the scanning number increases higher than 15 (as shown in Fig. 6d), anti-reflection structures generated by laser ablation are over etched and anti-reflection performance becomes poorer. More applications can be considered in the field of electrochemical fuel generation [18] and biological field [35, 36] with such periodic surface structures.

4. Conclusions

Nanosecond-laser ablation of c-Si immersed inside liquids shows the formation of high aspect ratio anti-reflection structures. Light trapping with feature size larger than wavelength is due to high aspect ratio structures. The fabrication of periodic conical structures is realized via proper laser scanning gap. The strong plasma produced by laser is limited with liquids. Wider and deeper craters are created under the action of the high temperature and high pressure plasma. With a good heat transfer property of liquid, HAZ is greatly reduced and the structure melting recasting is effectively avoided. Laser ablation with liquid assistance is verified as an efficient method to fabricate high aspect ratio structures. The average reflection of 3.28% over a wavelength range from 380 to 780 nm and anti-reflection structures with 5.01 aspect ratio are realized for laser ablation inside water. The enhancement of aspect ratio and the improvement of processing rate are also devoted to localized chemical etching inside NaOH solution (wt=20%). This provides a novel way for the applications of high efficient fabrication of the ARS.

Acknowledgments

This work is funded by Fujian Provincial Science and Technology Program (No. 2020H0006), National Natural Science Foundation of China (No. 62175203), Innovation Laboratory for Sciences and Technologies of Energy Materials of Fujian Province Applied Research Project (No. RD2020050301).

References

[1] N. Lu, Q. Lei, X. Xu, L. Yang, Z. Yang, Z. Liu, Y. Zeng, J. Ye, and S. He: Opt. Express, 30, (2022) 21309.

[2] J.W. Leem, Y.M. Song, and J.S. Yu: Nanoscale, 5, (2013) 10455.

[3] Y. Zhang, B. Jia, and M. Gu: Opt. Express, 24, (2016) A506.

[4] Z. Han, Z. Jiao, S. Niu, and L. Ren: Progress in Mater. Sci., 103, (2019) 1.

[5] Y. Li, Y. Li, L. Chen, and M. Hong: Opto-Electron. Eng., 44, (2017) 313.

[6] J. Li, J. Zhu, and X. Gao: Small, 10, (2014) 2578.

[7] J. Morikawa, M. Ryu, G. Seniutinas, A. Balcytis, K. Maximova, X. Wang, M. Zamengo, E.P. Ivanova, and S. Juodkazis: Langmuir, 32, (2016) 4698.

[8] G. Zyla, A. Kovalev, M. Grafen, E.L. Gurevich, C. Esen, A. Ostendorf, and S. Gorb: Sci. Rep., 7, (2017) 17622.

[9] K. Li, R. Wu, Y. Ruan, L. Zhang, and H. Zhen: Sol. Energy, 170, (2018) 800.

[10] Z. Huang, C. Cai, L. Kuai, T. Li, M. Huttula, and W. Cao: Sol. Energy, 159, (2018) 733.

[11] F. Teng, N. Li, L. Liu, D. Xu, D. Xiao, and N. Lu: RSC Adv., 6, (2016) 15803.

[12] A. Smyrnakis, E. Almpanis, V. Constantoudis, N. Papanikolaou, and E. Gogolides: Nanotechnology, 26, (2015) 085301.

[13] M.-D. Ko, T. Rim, K. Kim, M. Meyyappan, and C.-K. Baek: Sci. Rep., 5, (2015) 11646.

[14] P. Mokarian-Tabari, R. Senthamaraikannan, C. Glynn, T.W. Collins, C. Cummins, D. Nugent, C. O'Dwyer, and M.A. Morris: Nano Lett., 17, (2017) 2973.

[15] Y.-Y. Chou, K.-T. Lee, and Y.-C. Lee: Appl. Surf. Sci., 377, (2016) 81.

[16] J. Yang, F. Luo, T.S. Kao, X. Li, G.W. Ho, J. Teng, X. Luo, and M. Hong: Light Sci. Appl., 3, (2014) e185.

[17] L. Chen and M. Hong: Opto-Electron. Sci, 1, (2022) 210007.

[18] C.S. Saraj, S.C. Singh, G. Verma, R.A. Rajan, W. Li, and C. Guo: Opto-Electron. Adv., 5, (2022) 210105.

[19] S. Zhu, Y.F. Lu, and M.H. Hong: Appl. Phys. Lett., 79, (2001) 1396.

[20] P. Maack, A. Kanitz, J. Hoppius, J. Koehler, C. Esen, and A. Ostendorf: Proc. SPIE., Vol. 11989, (2022) 119890L.

[21] Z. Zhai, W. Wang, X. Mei, K. Wang, and H. Yang: Opt. Commun., 390, (2017) 49.

[22] M.H. Hong, K.Y. Ng, Q. Xie, L.P. Shi, and T.C. Chong: Appl. Phy. A: Mater. Sci. Process., 93, (2008) 153.

[23] J. Lam, J. Lombard, C. Dujardin, G. Ledoux, S. Merabia, and D. Amans: Appl. Phys. Lett., 108, (2016) 074104.

[24] M.E. Shaheen, J.E. Gagnon, and B.J. Fryer: J. Appl. Phys., 113, (2013) 213106.

[25] A. Hayat, S. Bashir, M. Akram, K. Mahmood, and M.H. Iqbal: Appl. Surf. Sci., 357, (2015) 2415.

[26] Z. Lian, J. Xu, Z. Yu, P. Yu, W. Ren, Z. Wang, and H. Yu: ACS Appl. Mater. Interfaces, 12, (2020) 6573.

[27] M.Y. Shen, C.H. Crouch, J.E. Carey, and E. Mazur: Appl. Phys. Lett., 85, (2004) 5694.

[28] B. Kumar and R.K. Thareja: Phys. Plasmas, 19, (2012) 033516.

[29] M. Aghaei, S. Mehrabian, and S.H. Tavassoli: J. Appl. Phys., 104, (2008) 053303.

[30] Y. Liao, Y. Yang, and G.J. Cheng: J. Trans. ASME, Ser. B, 134, (2012) 034503.

[31] F. Luo, Y. Guan, W. Ong, Z. Du, G. Ho, F. Li, S. Sun, G. Lim, and M. Hong: Opt. Express, 22, (2014) 23875.

[32] J. Yang, J. Li, Z. Du, Q. Gong, J. Teng, and M. Hong: Sci. Rep., 4, (2014) 06657.

[33] T. Baum and D.J. Schiffrin: J. Electroanal. Chem., 436, (1997) 239.

[34] K. Laidler: World Phys. Chem., (1993) 188.

[35] Y. Zhang, S. Jiang, Y. Hu, T. Wu, Y. Zhang, H. Li, A. Li, Y. Zhang, H. Wu, Y. Ding, E. Li, J. Li, D. Wu, Y. Song, and J. Chu: Nano Lett., 22, (2022) 2923.

[36] A. Li, H. Li, Z. Li, Z. Zhao, K. Li, M. Li, and Y. Song: Sci. Adv., 6, (2020) eaay5808.

(Received: January 23, 2023, Accepted: April 2, 2023)